THESIS FOR THE DEGREE OF LICENTIATE OF ENGINEERING

Selective Catalytic Reduction of NO_x over Alumina-Supported Silver and Indium during Lean Operation

LINDA STRÖM

Department of Chemistry and Chemical Engineering
CHALMERS UNIVERSITY OF TECHNOLOGY
Göteborg, Sweden 2016

Selective Catalytic Reduction of NO_x over Alumina-Supported Silver and Indium during Lean Operation
LINDA STRÖM

Licentiatuppsatser vid instutitionen för kemi och kemiteknik. 2016:02
ISSN: 1652-943X

Applied Surface Chemistry
Department of Chemistry and Chemical Engineering
Chalmers University of Technology
SE-412 96 Göteborg
Sweden

Telephone: +46 (0)31-772 1000

Chalmers Reproservice
Göteborg, Sweden 2016

Selective Catalytic Reduction of NO_x over Alumina-Supported Silver and Indium during Lean Operation

Linda Ström
Applied Surface Chemistry
Department of Chemistry and Chemical Engineering
Chalmers University of Technology

ABSTRACT

Catalytic emission control for vehicles was first applied in the 1970's. The first such catalysts were designed to oxidize unburned hydrocarbons (HC) and carbon monoxide (CO). A few years later, the oxidation catalyst was further developed into the three-way catalyst (TWC), which efficiently removes CO, HC and nitrogen oxides (NO_x), under stoichiometric air-to-fuel ratios. However, the awareness of climate changes, caused by anthropogenic emissions of carbon dioxide (CO_2), is a major motivator for the development of fuel-efficient engines, operating in excess oxygen (lean) combustion. At these air-to-fuel ratios, the TWC is ineffective for NO_x reduction, promoting the development of lean NO_x reduction techniques. Among the most promising today is selective catalytic reduction (SCR), for which the silver-alumina (Ag/Al_2O_3) catalyst shows promising results, both with HC and ammonia (NH_3), as the reducing agent.

The current work focuses on the nature of the active sites of the Ag/Al_2O_3 catalyst and the impact of the structure of the reductant on the selective catalytic reduction of NO_x. For this purpose, five different hydrocarbons and oxygenates, all containing two carbon atoms in the structure, as well as NH_3, are investigated as reducing agents, with and without the presence of hydrogen. Furthermore, the influence of the active phase is elucidated by exchanging silver for the equivalent molar amount of indium. The catalysts are prepared by incipient wetness impregnation, characterized with regard to specific surface area, crystalline structure, concentration and strength of acidic sites, SCR activity and surface species. The latter are studied by diffuse reflectance ultraviolet-visible (UV-vis) spectroscopy, where spectra from both the fresh samples and from samples subjected to various gas-phase pretreatments, mimicking conditions of the SCR reaction environment, are recorded. The connection between the silver and indium species, and the gas-phase environment is discussed, and it is proposed that species important for the activation of the reducing agent are essential for high SCR activity, both during HC- and NH_3-SCR.

Furthermore, quantification of the NO reduction and NH_3 slip over Ag/Al_2O_3 is performed for different locations of the reductant injection spray. The probability of a stoichiometric ammonia dose is higher when the spray is positioned in the center of the exhaust pipe, compared to at the pipe wall. Moreover, the NO conversion increases rapidly with increasing ammonia dose, however, NH_3 doses of several times the stoichiometric amount do not improve NO reduction significantly but increase the NH_3 slip almost linearly.

Keywords: Lean NO_x reduction, HC-SCR, NH_3-SCR, silver, indium, alumina

List of papers

I. **Hydrogen-assisted SCR of NO_x over alumina-supported silver and indium catalysts using C_2-hydrocarbons and oxygenates**
Linda Ström, Per-Anders Carlsson, Magnus Skoglundh & Hanna Härelind
Applied Catalysis B: Environmental **181** (2016) 403-412

II. **On the hydrogen effect in NH_3-SCR of NO_x over alumina-supported silver and indium catalysts**
Linda Ström, Per-Anders Carlsson, Magnus Skoglundh & Hanna Härelind
In manuscript

III. **Quantification of urea-spray non-uniformity effects on the H_2-assisted NO reduction and NH_3 slip over an Ag/Al_2O_3 catalyst**
Linda Ström, Henrik Ström, Andreas Darnell, Per-Anders Carlsson, Magnus Skoglundh & Hanna Härelind
Energy Procedia **75** (2015) 2317-2322

Contribution report

I. I prepared the catalysts, performed all experimental work, interpreted the results together with my co-authors, wrote the first draft of the manuscript and was responsible for writing and submitting the manuscript.

II. I prepared the catalysts, performed all experimental work, interpreted the results together with my co-authors and wrote the first draft of the manuscript.

III. I prepared the catalysts, performed all experimental work, interpreted the results together with my co-authors, wrote the first draft of the manuscript and was responsible for writing and submitting the manuscript.

List of abbreviations

Ag/Al_2O_3	Silver-alumina
BET	Brunauer-Emmett-Teller, adsorption isotherm for determination of surface areas of solids
CEM	Controlled evaporator mixer
CFD	Computational fluid dynamics
C/N	Ratio between the number of carbon and nitrogen atoms
CO	Carbon monoxide
CO_2	Carbon dioxide
DME	Dimethyl ether
FTIR	Fourier transform infrared spectroscopy
HC	Hydrocarbons
In/Al_2O_3	Indium-alumina
N_2	Nitrogen
N_2O	Nitric oxide
NH_3	Ammonia
NO_x	Nitrogen oxides (NO and NO_2)
NSR	NO_x storage and reduction
PGM	Platinum group metals
PM	Particulate matter
SCR	Selective catalytic reduction
SO_x	Sulfur oxides (SO_2 and SO_3)
TPD	Temperature programmed desorption
TWC	Three-way catalyst
UV-vis	Ultraviolet and visible
XRD	X-ray diffraction

Contents

Chapter 1

Introduction

1.1 The development of emission control

Today, the transport sector is the most important source to air pollutions in the western world. Among these emissions are carbon monoxide (CO), hydrocarbons (HC), particulate matter (PM), sulfur oxides (SO_x) and nitrogen oxides (NO_x). The latter (almost exclusively NO) is, regardless of the chemical composition of the fuel, formed during combustion at high temperatures and is oxidized into NO_2 in the atmosphere. This suffocating gas is largely responsible for the brownish color of smog and plays a major role in the formation of ground-level ozone. In the environment, this strongly oxidizing agent reacts in the air to form nitric acid as well as toxic organic compounds, which cause acidification and eutrophication [1]. Moreover, in the human body, NO_x can irritate the lungs and lower resistance to respiratory infections, such as influenza. The effect of short-term exposure is still unclear, however, long-term frequent exposure to concentrations higher than typically found in the ambient air, may cause increased incidence of acute respiratory illness [1]. On a global basis, it is estimated that 500.000 people die each year as a result of the air pollutions from the transport sector [2]. In Europe, the average pollution of NO_x was 16.2 kg per capita in 2013, of which the largest source was road transportation (39.4%) [3], see Figure 1.1.

Catalytic emission control has been applied to passenger cars in the US since 1975. The first generation of car exhaust catalysts was able to oxidize unburned HC and CO. In 1981, a new catalytic system called the three-way catalyst (TWC) was developed, which operates under stoichiometric conditions and, except for CO and HC, also converts NO_x [2] (see Figure 1.2). Gasoline powered vehicles operate under stoichiometric conditions and emissions provided by this type of engine can be effectively converted by

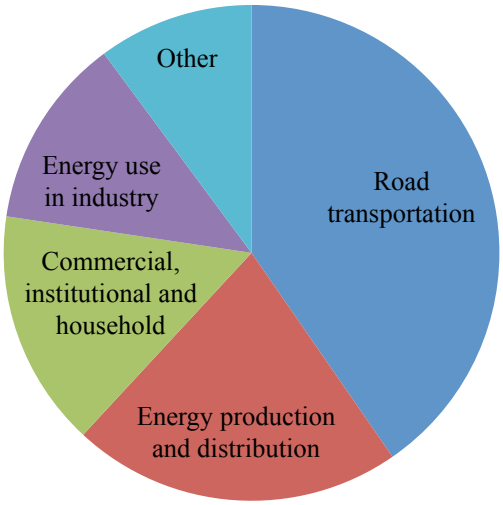

Figure 1.1: NO_x emissions divided by source sector in the EU in 2013 [3].

the TWC. However, the awareness of climate changes, caused by anthropogenic emissions of carbon dioxide (CO_2), has gained increased concerns, motivating the development of more fuel-efficient engines, operating under lean conditions (excess oxygen) and in this way emitting less CO_2 per driven km, compared to the ordinary gasoline engine. However, lean conditions contradict the fundamentals of the TWC, hence another abatement technique is required for reducing NO_x under lean conditions. The legislation regarding NO_x emissions was first applied in Europe 1992 by the Euro I standards. Since then, the standards have been updated several times and Euro VI requires nowadays NO_x emissions of no more than 0.4 g/kWh. The development of Euro-standards of NO_x emissions is shown in Figure 1.3.

Promising techniques for lean NO_x reduction at present involves NO_x storage and reduction catalysts and selective catalytic reduction with hydrocarbons (HC-SCR) or ammonia (NH_3-SCR). A promising catalyst for HC-SCR is silver-alumina (Ag/Al_2O_3) [5-9], which shows high stability under hydrothermal conditions [10].

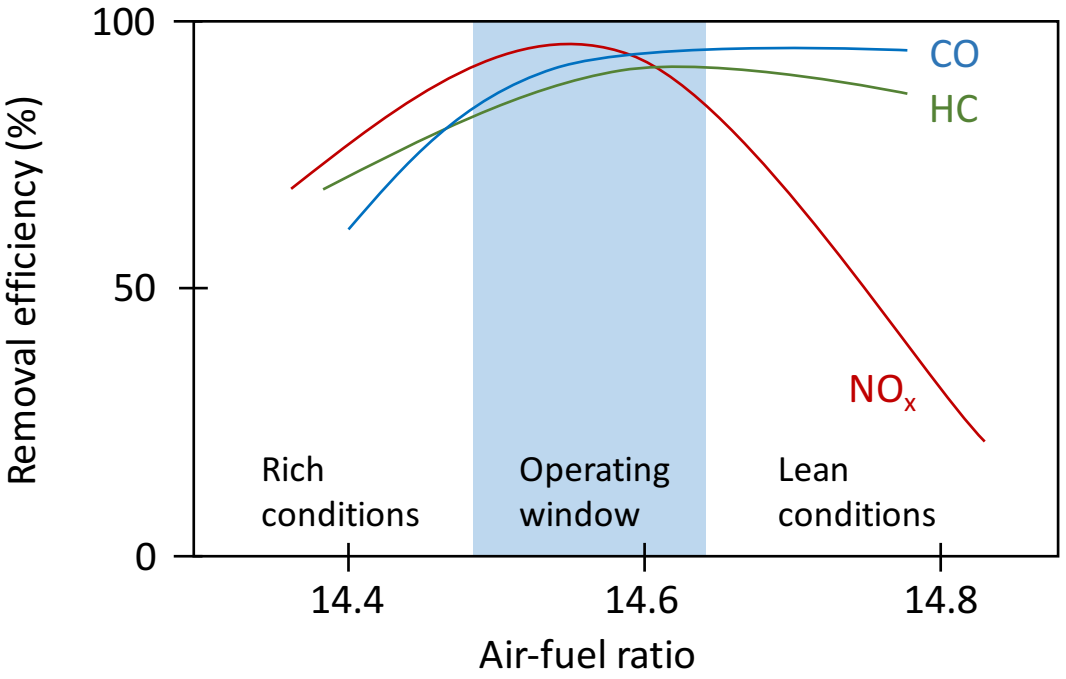

Figure 1.2: Illustration of the catalytic conversion of CO, unburned hydrocarbons and NO_x as a function of air-to-fuel ratio, over the TWC.

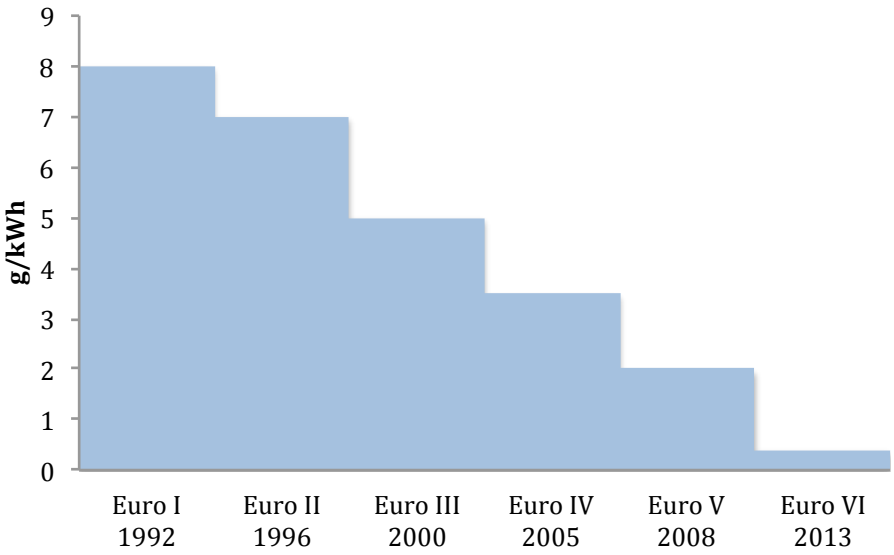

Figure 1.3: The historical development of Euro emission standards for NO_x emission for heavy-duty vehicles. Data for this chart is collected from Ref. [4].

1.2 Objectives

The aim of this work is to study the nature of the active sites of the Ag/Al_2O_3 catalyst and the impact of the structure of the reductant on the lean NO_x reduction over alumina-based silver and indium catalysts. For this purpose, a Ag/Al_2O_3 catalyst is compared to an In/Al_2O_3 catalyst containing the same molar amount of active phase, using various C_2-hydrocarbons and oxygenates (paper I), and H_2-assisted NH_3 (paper II), as reductants. The connections between the gas-phase environment, and type of silver and indium species in the samples are investigated using UV-vis spectroscopy (paper I & II). Furthermore, the impact of the location of the urea spray injection on NO reduction and ammonia slip in H_2-assisted NH_3-SCR is quantified (paper III).

Chapter 2

Background

2.1 Challenges associated with lean NO_x reduction

Development of lean NO_x reduction catalysts for usage in vehicles involves several challenges. For example, the engine operates under transient loading, which results in variations in temperature and flow rate of the exhaust stream over time. Hence, a successful catalyst should be able to operate properly over a wide temperature range and exhaust flow rate. During lean operation in energy-efficient engines, such as the diesel engine, the exhaust temperature is considerably lower compared to the stoichiometric gasoline engine, around 150-250°C in light-duty exhaust and 100-200°C in heavy-duty [11]. The lean NO_x reduction catalyst must therefore be able to operate effectively at low temperatures. Furthermore, the catalyst is subjected to small amounts of electronegative elements such as sulfur and phosphorus, which tend to adsorb strongly to the surface and poison the catalyst by physical or electronic blockage of active sites [12]. Another degradation mechanism is sintering, of the active phase, which leads to loss in surface area and increase in the average surface coordination. Formation of volatile compounds, containing the active phase, also contributes to catalyst depletion, as well as fouling of pores. In addition to these demands on a successful lean NO_x reduction catalyst to provide high activity at low temperature and to avoid degradation, space limitations onboard a vehicle need to be considered. Some of today's promising techniques are presented in Section 2.2.

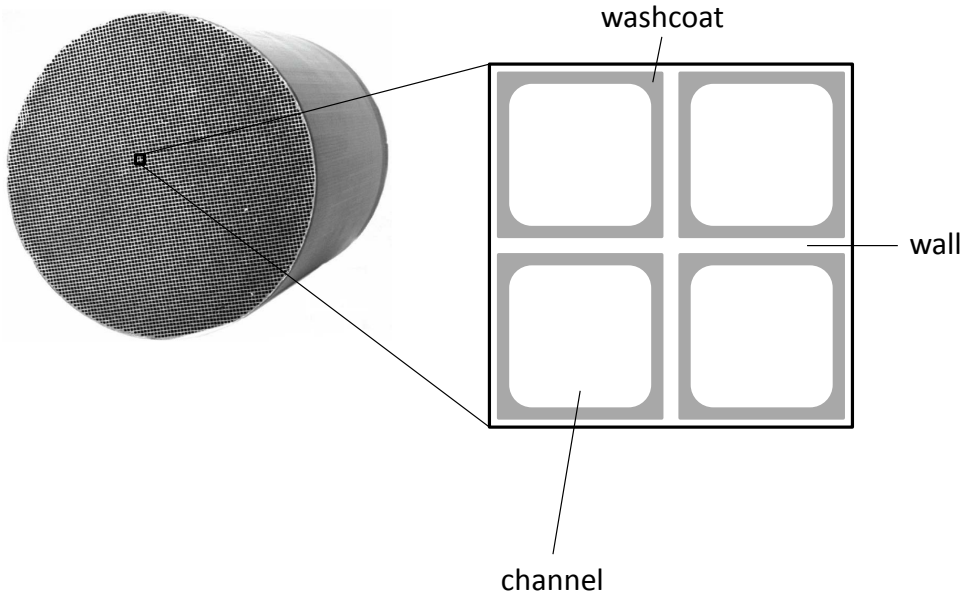

Figure 2.1: A schematic illustration of a monolithic reactor with the entrance of four individual channels enlarged. The washcoat consists of the porous support material and the catalytically active phase.

2.2 Methods for conversion of NO_x

Today, the standard of vehicle emission control is monolithic reactors, typically made of a porous ceramic substrate material such as cordierite, but can also be metallic. The ceramic substrate consists of thousands of channels and is coated with the catalytic material, which consists of a porous support material, in order to provide a large surface area, and the active phase. Figure 2.1 shows a typical monolithic catalyst. In this section, some of the promising techniques for lean NO_x reduction is presented.

2.2.1 NO_x storage and reduction

A promising technique for lean NO_x reduction is NO_x storage and reduction (NSR), where Pt and BaO supported by Al_2O_3 is the most commonly used catalytic material. In this approach, NO is first oxidized to NO_2 over Pt and subsequently adsorbed as stable nitrite or nitrate species on the storage material BaO during a lean phase, which lasts for 1-2 minutes. During a subsequent rich (oxygen deficiency) period of 3-5 seconds, the trapped NO_x is released and reduced to N_2 by unburned fuel and CO over Pt [13-15]. Drawbacks of this technique include the complexity of the engine system and fuel penalty during the rich periods [16]. Also, the formation of stable

sulfates with the NO_x-storage material and the oxide support makes the NSR-catalyst degrade over time, and in requirement of regeneration, which is usually performed under high temperatures (>600 °C) and during the rich part of the cycle [17].

2.2.2 Hydrocarbon-SCR

Another feasible solution for lean NO_x reduction is selective catalytic reduction using hydrocarbons (HC-SCR) [7, 18-23]. In this approach, the hydrocarbon-based fuel is injected into the exhaust system upstream the SCR catalyst and used as reducing agent for NO_x over the catalyst. An advantage of using the fuel as the reductant is that there is no need for an additional tank for reductant storage onboard the vehicle, and thereby being a NO_x reduction system that is not limited to heavy-duty vehicles. However, some of the challenges regarding this technique are to receive high conversion of NO_x with high selectivity to N_2 despite high oxygen concentration, low temperature, transient loadings and exposure to sulfur and water.

The exact reaction scheme of lean NO_x reduction with hydrocarbons is still under debate. However, some general differences have been detected over different types of catalysts, based on noble metals, oxides or zeolites. The TWC is based on various combinations of noble metals such as Pt, Pd and Rh as the active phase and converts HC, CO and NO_x effectively under stoichiometric conditions at 400-800°C. Since this catalyst proved to be completely ineffective for NO_x reduction during large excess of oxygen, the platinum group metals (PGMs) were first assumed to be incapable of reducing NO_x in lean conditions. However, although PGM-based catalysts are ineffective at moderate or high temperatures, they have showed to be active for NO_x reduction at low temperatures (typically below 300°C) [18]. Reaction mechanisms proposed for lean NO_x reduction by short-chained alkene-type hydrocarbons over Pt are *i*) the intermediacy of cyanide or isocyanate surface species, *ii*) the intermediacy of organo-nitro species and *iii*) decomposition of NO followed by oxygen removal by the HC [18].

NO adsorbs as strongly bound nitrite and nitrate species in excess oxygen (but adsorbs only weakly in absence of oxygen) on most catalyst surfaces [24]. Over oxide catalysts, the first step in the reaction mechanism is proposed to be the surface adsorption of NO_x. Adsorbed oxidized hydrocarbon species, such as acetate [22, 25], are formed during SCR with various hydrocarbons or oxygenates over alumina-based catalysts, and are believed to react with the adsorbed NO_x species, yielding organo-nitrogen species, which appears to be the rate-determining step [18]. Via these species, reduced nitrogen species, such as –NCO and NH_3 can be formed. It has been proposed that

the nitrogen coupling to form N_2 could occur by a reaction between these reduced species and NO(g) or adsorbed NO_x [18, 26].

2.2.3 NH_3-SCR

NH_3-SCR is an already implemented technique for the reduction of NO_x on heavy-duty vehicles such as buses and trucks [27]. Traditional active metal oxides used in NH_3-SCR are V_2O_5, WO_3 and MoO_3 [15], where the vanadium-based catalyst is the most active for lean NO_x removal. However, usage of this highly toxic catalyst poses some serious problems involving high vapor pressure of vanadium oxides that might form volatile vanadia species leading to toxic emissions [28], which calls for new types of catalytic materials. To avoid storage and handling issues of ammonia, the reductant is injected to the exhaust system as a urea-water solution, which decomposes to ammonia over the catalyst. Alumina has been shown to be especially suitable for this decomposition [28]. However, there are some disadvantages regarding NH_3-SCR, such as distribution of the urea solution and the possibility that unreacted ammonia is emitted (so called ammonia slip) [29].

2.3 Alumina-supported catalysts

2.3.1 The Ag/Al_2O_3 catalyst

Alumina-supported catalysts have received much attention thanks to their high stability under hydrothermal conditions. The alumina phase most widely used for this purpose is the porous and amorphous γ-Al_2O_3, which provides a high surface area (100-300 m^2/g). This support material is prepared by calcination of Boehmite (AlO(OH)) or Bayerite/Gibbsite ($Al(OH)_3$) at 500-850°C.

Miyadera was the first reporting on alumina-supported silver (Ag/Al_2O_3) catalysts in 1993 [30]. Ever since, a major interest has been directed towards this catalyst, which exhibits SCR activity both with ammonia [31-35] and hydrocarbons [21, 30, 36-38]. The optimal silver loading has been frequently studied and it has been found to be around 2 wt% for impregnated catalysts [8, 22, 26, 39, 40]. The reason for this has been suggested to involve the optimal silver density, which should be close to 0.7 Ag/nm^2 [41].

The species active for SCR of NO_x has been suggested to be Ag^+-ions [22, 42, 43] and small clusters of ionic silver ($Ag_n{}^{\delta+}$, $n \leq 8$) [32, 43], or a combination of these. Metallic silver particles are most likely active for total oxidation of the reductant by molecular oxygen [26]. Moreover, it has

also been suggested that active sites of Ag/Al_2O_3 vary as a function of the reductant type and reaction temperature [23]. Over Ag/Al_2O_3, the following reactions are proposed to be involved: *i*) oxidation of NO to NO_2 followed by the formation of surface nitrites and nitrates, *ii*) adsorption and partial oxidation of hydrocarbons, and *iii*) surface reactions between the adsorbed nitrogen species and the partially oxidized hydrocarbons [14].

The 'hydrogen effect'

That the addition of small amounts of hydrogen to the gas feed majorly promotes the NO_x reduction activity over the Ag/Al_2O_3 catalyst was first discovered by Satokawa [44], and has later been widely studied [7, 33, 41, 45]. The effect is reversible so that addition/removal of hydrogen from the feed increases/decreases the SCR activity instantly. Such cycles can be repeated without loss in catalytic performance [7, 43]. Moreover, the mechanism(s) behind this promotion has been widely debated. Suggestions involve reduction of adsorbed nitrogen species [45-48], enhanced activation of the hydrocarbon in HC-SCR [32, 43, 48-50], modification of the Ag-species [32, 43, 48, 49], as well as direct effects on the reaction mechanism [48, 51]. During NH_3-SCR, Ag/Al_2O_3 lacks in activity without the presence of hydrogen in the feed while NO_x is completely converted at relatively low temperatures when hydrogen is present [31]. In/Al_2O_3 has shown a minor hydrogen effect during NH_3-SCR [52].

2.3.2 The In/Al_2O_3 catalyst

Alumina-supported indium has been studied as an SCR catalyst, both with NH_3 [52] and hydrocarbons [20, 53-55]. This catalyst has shown relatively high activity in the presence of water, and a catalyst prepared by the sol-gel method shows higher activity than that by impregnation [56]. Park et al. [57] proposed that, during HC-SCR, well-dispersed indium oxide clusters provide hydrocarbon activation that, with utilization of active alumina sites, selectively reduce NO_x to N_2.

Chapter 3

Scientific methods

3.1 Catalyst preparation and monolith coating

The catalysts evaluated in this work have been prepared by incipient wetness impregnation of γ-Al_2O_3 (PURALOX® SBa 200, Sasol) using silver nitrate ($\geq$ 99.0% Sigma-Aldrich) for the Ag/Al_2O_3 sample and indium nitrate hydrate (99.99% Sigma Aldrich) for the In/Al_2O_3 sample. In this preparation method, the pore volume of the support material (in this case γ-Al_2O_3) is determined by slowly adding drops of water that migrate into the pores. When the support is saturated the powder attains a creamy consistence. The active phase precursor is dissolved in a volume of water that corresponds to the pore volume of the support material and the precursor solution is added to the support. The Ag loading was 2.0 wt% and the In loading corresponded to the equivalent molar amount, giving an In loading of 2.1 wt%. After the addition of precursors, the powder samples were frozen by liquid nitrogen subsequent to the impregnation, then freeze-dried and finally calcined in air at 600°C for four hours.

Monoliths with 188 channels (400 CPSI, $\varnothing = 20$ mm, L = 20 mm) were cut from a commercial cordierite honeycomb structure (Corning) and calcined in air at 600°C for one hour. Washcoat slurries were prepared, containing binder agent (DISPERAL® P2, Sasol) and one of the powder catalysts (ratio 1:4) in 1:1-ratio ethanol-water solutions. Monoliths were dipped into the slurries, gently shaken for removal of excess slurry, dried in a 90°C hot air stream and subsequently calcined at 500°C for 3 minutes. The coating procedure was repeated until the washcoat mass corresponded to 20% of the coated monolith mass. Finally, the monoliths were calcined in air at 600°C for one hour. A coated monolith sample is shown in Figure 3.1.

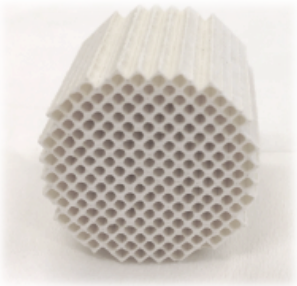

Figure 3.1: A monolith coated with Ag/Al_2O_3.

3.2 Characterization techniques

3.2.1 Specific surface area according to the BET-method

The specific surface area of a solid material can be determined according to the method published in 1938 by Brunauer, Emmett and Teller [58] (the BET-method). The technique is based on physical adsorption of an inert gas (most often nitrogen) on the surface of the solid material. Generally, the method provides reliable values of the surface area, unless the sample involves micropores, where the size of the pores in the adsorbent and the adsorbate is similar [59]. The method assumes that *i*) the heat of adsorption of the first monolayer is constant, *ii*) the lateral interaction of the adsorbate is negligible, *iii*) the adsorbed molecules can act as new adsorption surface and the process can repeat itself and *iv*) the heat of adsorption of all monolayers but the first is equal to the heat of condensation [60]. In practice, the sample is first heated up under vacuum to remove moisture and subsequently cooled down to 77 K by liquid nitrogen. At this temperature N_2 is dosed in small volumes and the pressure is allowed to stabilize. The physisorbed volume of N_2 can now be calculated using the ideal gas law. Knowing the area of one adsorbed N_2-molecule, the specific surface area of a sample can be derived from the following formula:

$$\frac{P}{V(P_0 - P)} = \frac{1}{V_\mathrm{m}C} + \frac{C-1}{V_\mathrm{m}C}\frac{P}{P_0} \tag{3.1}$$

where P is the equilibrated partial pressure, V is the volume of absorbed gas, P_0 is the saturation pressure and V_m is the inert gas monolayer volume. At low pressure, the relationship between $P/V(P_0 - P)$ and P/P_0 is linear, hence it follows that $1/V_\mathrm{m}C$ is where the straight line intercepts the y-axis and $(C-1)/(V_\mathrm{m}C)$ is the slope of the line.

In Paper I, II and III, N_2 sorption according to the BET-method was

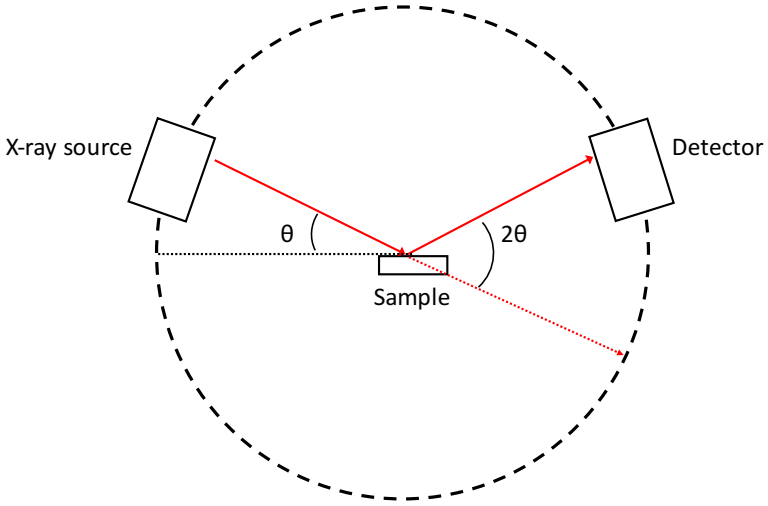

Figure 3.2: Illustration of an X-ray diffraction experiment.

used to determine the specific surface area of the powder catalyst samples using a Micrometrics TriStar® 3000 instrument.

3.2.2 X-ray diffraction – Crystal structure

The non-destructive technique X-ray diffraction (XRD) can be used to examine the crystal phase of a sample. When irradiated by X-rays with the wavelength λ, electron clouds of the crystal-structured atoms scatter the X-rays, which are measured by a detector. The distance between the lattice planes, d, can then be calculated by Bragg's law:

$$n\lambda = 2d \sin \Theta \tag{3.2}$$

Where n is any integer and Θ the incident angle.

The crystal phases of the catalysts were investigated using XRD (Siemens D5000 X-ray diffractometer scanning 2Θ from 5 to 65° in the scan mode 0.02°, 1 s) with Ni-filtered Cu $\kappa\alpha$ radiation. XRD was used in Paper I and II. An illustration of the technique is presented in Figure 3.2.

3.2.3 NH_3-TPD – Surface acidity

The density and strength of the acidic sites of a catalytic sample can be characterized by temperature programmed desorption (TPD) of NH_3. In this work, the flow reactor described in section 3.3 was used for this experiment.

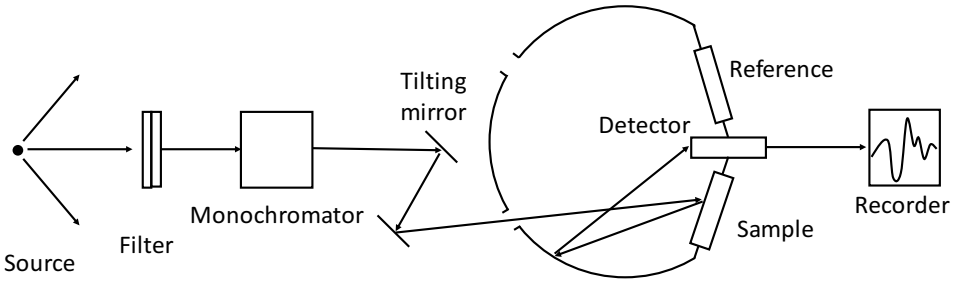

Figure 3.3: A schematic diagram of a UV-vis spectrometer operating in the diffuse reflectance mode. Adapted from Ref. [61].

Prior to the NH_3 adsorption, the sample is pretreated to remove possible carbonaceous matter. By saturating the catalytic sites by this strong base at low temperature (around 100°C) and then slowly increase the temperature, the amount of NH_3 able to chemisorb to the sites at low temperature is desorbed and can be measured. Weakly adsorbed NH_3 is released first and more strongly bound at somewhat higher temperatures, which gives the possibility to distinguish between different kinds of acidic sites. NH_3-TPD was used in paper I, II and III.

3.2.4 UV-visible diffuse reflectance spectroscopy – Surface species

Electronic *d-d* transitions are observable in the ultraviolet and visible light region (200-2000 nm) when degenerated *d* orbitals are split by placing a transition metal ion in a crystal field. Furthermore, the number of *d*-electrons, the effective charge on the ion and the distribution and charge of the surrounding anions are circumstances that affect the spread of the energy levels [61]. Consequently, the technique can be used for characterization of the types of species present in a solid sample. A typical beam path is visualized in Figure 3.3.

In this study, UV-vis was used to characterize the oxidation states of the samples studied in Paper I and II, where spectra have been deconvoluted into Gaussian peaks. Spectra in the range 200-1500 nm were recorded using a Varian Cary 5000 UV-vis-NIR spectrophotometer equipped with an external DRA-2500 unit. The reflectance spectra were recorded and the spectrum of the Al_2O_3 support was subtracted as part of the background. To investigate the influence of reaction conditions on the type of surface species, both fresh catalysts and samples exposed to various gas-phase pretreatments, using the flow reactor described below (3.3), were analyzed.

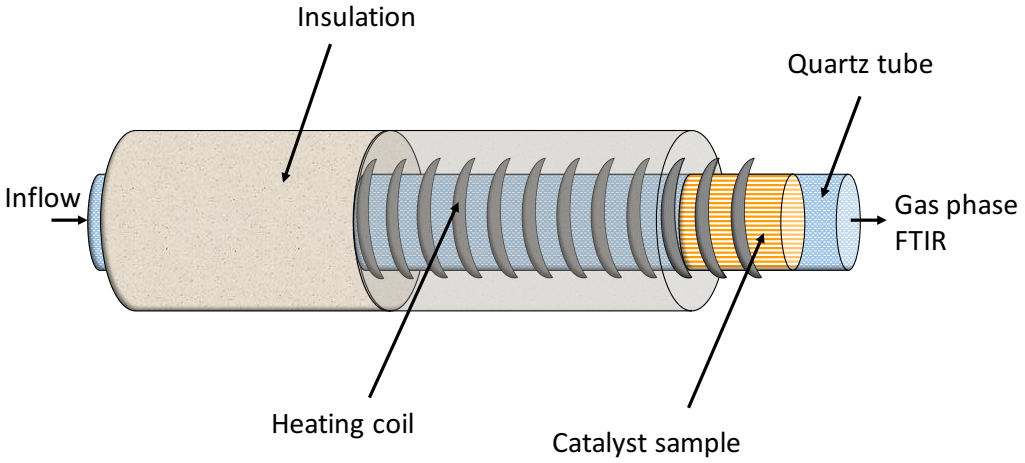

Figure 3.4: Illustration of the flow reactor used in the NO_x-reduction experiments, UV-vis pretreatments and for the NH_3-TPD.

3.3 Flow reactor experiments

The catalytic activity for lean NO_x reduction was evaluated during extinction ramps (500 to 100°C by 10°C/min), using a flow reactor illustrated in Figure 3.4. The reactor chamber consists of an insulated horizontal quartz tube (L = 80 cm, $\varnothing_i$ = 22 mm) heated by a metal coil. The catalyst temperature is measured inside the sample and the reactor temperature is controlled 15 mm before the catalyst sample by K-type thermocouples. Uncoated monoliths placed before and after the coated monolith shield the thermocouple from heat radiation emitted by the heating coil as well as reduce axial radiation heat losses from the coated monolith sample [62]. The inlet feed gases are introduced and regulated by mass-flow controllers (Bronkhorst Hi-Tech) and the outlet gas flow is analyzed by a gas-phase FTIR spectrometer (MKS 2030). Fluent hydrocarbons/oxygenates and water are introduced to the reactor via a controlled evaporator mixer system (CEM, Bronkhorst Low ΔP Hi-Tech), carried by Ar.

The total gas flow was set to 3500 ml/min in all experiments, which corresponds to a space velocity (GHSV) of 33,400 h^{-1}. Prior to each measurement, the sample was pretreated in O_2 (10%, Ar balance) at 500°C for 30 min. In the HC-SCR study, the gas feed composition was 500 ppm NO, 1500 ppm C_2-hydrocarbon (C/N ratio of 6, in line with previous experience [35, 37]), 10% O_2 and 5% H_2O, in the presence or absence of 1000 ppm H_2. The C_2-

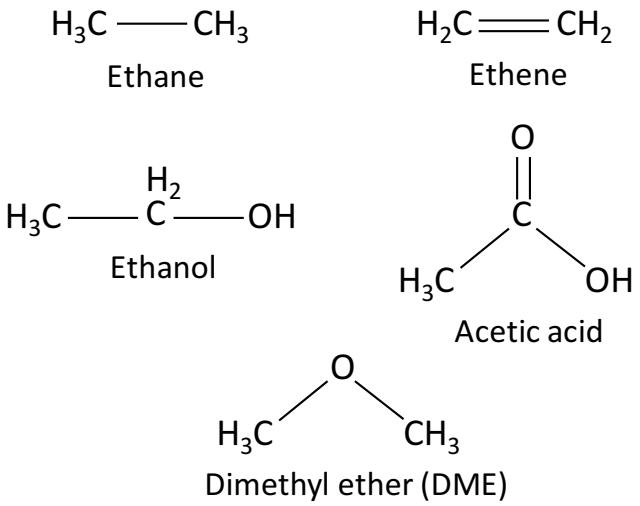

Figure 3.5: Structures of the hydrocarbons and oxygenates used as reductants.

hydrocarbons and oxygenates used are ethane, ethene, ethanol, acetic acid and DME, respectively, with the structures shown in Figure 3.5 (Paper I). In the NH_3-SCR study (paper II and III), the gas composition was 500 ppm NO, 500 ppm NH_3, 1000 ppm H_2, 10% O_2 and 5% H_2O.

In addition to lean NO_x reduction and NH_3-TPD experiments, this reactor setup was also used for the UV-vis pretreatments of Paper I and II, using a flow rate of 100 ml/min.

Chapter 4

Results and discussion

In the present work, Ag/Al_2O_3 has been evaluated as an SCR catalyst with hydrocarbons and oxygenates, as well as ammonia, as reductants. During these experiments, the gas feed contained 500 ppm NO, 1500 ppm HC or 500 ppm NH_3, 10% O_2 and 5% H_2O. The experiments were performed in the presence or absence of 1000 ppm H_2 (Ar-balance). Furthermore, diffuse reflectance UV-vis spectra have been recorded after various pretreatments, elucidating the effect of the reaction environment on the catalyst surface species. In order to highlight the influence of the catalytic material on the NO_x-reduction activity, Ag/Al_2O_3 has been compared to an In/Al_2O_3 catalyst, holding the equivalent molar amount of active phase. The results and relating discussion of this work are presented in this section.

4.1 Influence of the reducing agent on lean NO_x reduction over Ag/Al_2O_3

The influence of the nature of the reducing agent on the lean NO_x reduction over Ag/Al_2O_3 was investigated using C_2-hydrocarbons and oxygenates (paper I), and NH_3 (paper II), with the results shown in Figure 4.1. The highest activity is achieved using hydrogen-assisted ethane as reductant. However, the other non-oxygenated hydrocarbon, ethene, starts reducing NO_x at somewhat lower temperature, compared to ethane, when hydrogen is absent. Among the oxygenated hydrocarbons, ethanol shows the highest NO_x reduction followed by acetic acid. With these reductants, the addition of hydrogen provides a shift in the activity window towards lower temperatures. Furthermore, DME lacks in activity both with and without hydrogen over this catalyst. Similarly, ammonia is totally inactive as reducing agent over Ag/Al_2O_3 when hydrogen is absent. However, in presence of hydrogen, am-

monia shows high activity already at low temperatures. The diversity in activity among these reductants demonstrates that the nature of the reducing agent is very important when designing a successful catalytic system. During HC-SCR, the current work demonstrates that NO_x reduction varies as a function of the structure of the reductant, since despite that all HC reductants are based on two carbon atoms, the activity for NO_x reduction differs significantly over the same catalyst. Parameters such as activation (i.e. partial oxidation) ability of the hydrocarbon, which in turn depends on the nature of the C-H (or C-C) bonds, accessibility of π-electrons, molecular orientation (steric effects) and sticking probability of the reductant have been identified as critical factors [38, 55, 56, 63, 64].

4.1.1 Influence of the gas-phase environment on the Ag phase

In order to investigate how the surface species of the Ag/Al_2O_3 catalyst are affected by the gas-phase environment, UV-vis spectra were recorded after various pretreatments. The Al_2O_3-subtracted UV-vis spectrum of the Ag/Al_2O_3 sample is shown in Figure 4.2. The spectrum has been deconvoluted using Gaussian peaks for identification purposes. Peaks in the range 200-260 nm are attributed to the $4d^{10}$ to $4d^9s^1$ transition of dispersed Ag^+ ions [42, 65-70]. However, it should also be noted that isolated Ag^+ ions exhibit peaks just below 200 nm [32, 71], which could not be detected due to instrument limitations. Furthermore, peaks in the range 238-370 are assigned to small $Ag_n{}^{\delta+}$ clusters ($n \leq 8$) [22, 67, 68, 72], and peaks above 390 nm are attributed to Ag^0 particles [22, 42, 68, 70, 73]. Hence, the UV-vis spectrum of the fresh Ag/Al_2O_3 sample shows that the sample contains a mixture of ions, clusters and metallic silver. Shimizu and Satsuma [23] demonstrated that the sites active for hydrocarbon activation varies as a function of the reaction conditions, especially with reductant type and temperature. During alkene-SCR, Ag^+-ions or Ag^+-containing species have been shown to provide hydrocarbon-activating sites. Alkanes exhibit lower activity compared to alkenes, and alkane-SCR therefore proceeds at higher temperatures, where $Ag_n{}^{\delta+}$ clusters provide active sites for hydrocarbon activation [23]. Furthermore, XRD diffractograms confirm that no particles larger than 3-5 nm of other crystalline phases than γ-Al_2O_3 are present in the sample [61]. Figure 4.3 shows that the impregnated silver sample is similar to the bare γ-Al_2O_3 sample, and that all peaks are characteristic for γ-Al_2O_3 [54, 74]. Moreover, the specific surface area, measured by N_2-sorption according to the BET method, shows that the surface area of the catalyst samples remains high

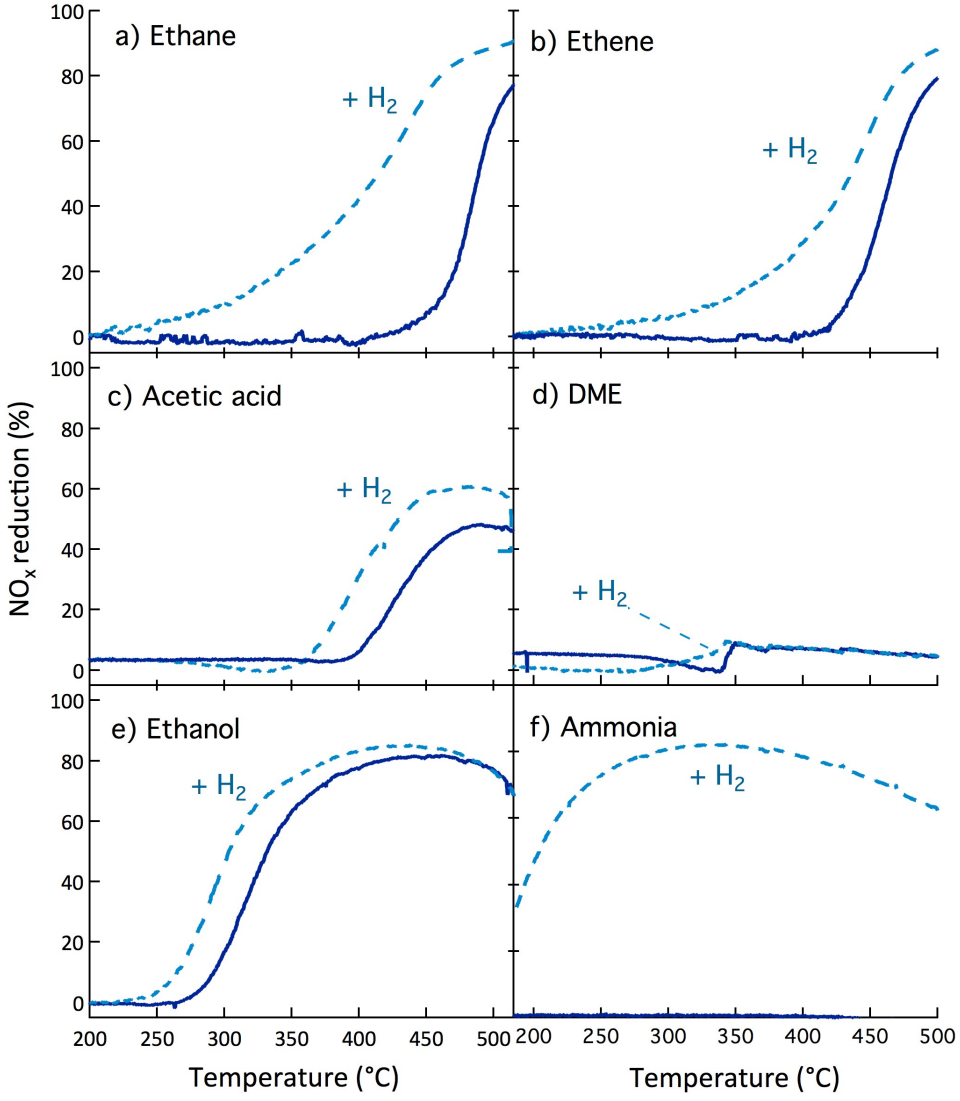

Figure 4.1: Lean NO_x reduction over Ag/Al_2O_3 as a function of the catalyst temperature using (a) ethane, (b) ethene, (c) acetic acid, (d) DME, (e), ethanol (1500 ppm HC-reductant) and (f) ammonia (500 ppm). Gas feed concentrations (except for the reductant): 500 ppm NO, 10% O_2, 5% H_2O, Ar-balance. Dotted lines represent the addition of 1000 ppm H_2 to the gas feed.

after impregnation (185, compared to 197 m^2/g of bare Al_2O_3).

As shown in the lean NO_x reduction experiments presented in Figure 4.1, the Ag/Al_2O_3 sample exhibits in general higher NO_x conversion when hydrogen is present in the feed gas mixture. UV-vis spectra recorded after hydrogen pretreatments at 200 and 300°C are shown in Figure 4.4, and clarifies that hydrogen exposure results in a change of surface species. Peaks at higher wavelengths (>260 nm) increase significantly, corresponding to increased concentration of silver clusters ($Ag_n^{\delta+}$) and metallic silver nanoparticles (Ag^0). The degree of reduction seems to increase with temperature since the pretreatment at 300°C results in a higher degree of totally reduced silver, compared to the pretreatment at 200°C. Moreover, during HC-SCR, an important reaction step has been identified as activation of the reductant by partial oxidation [14]. $Ag_n^{\delta+}$ clusters have been pointed out as sites active for this reaction step [43]. Hence, the concentration of sites identified as active for hydrocarbon activation increase with small amounts of hydrogen in the surrounding gas phase, which could be an origin to the 'hydrogen effect' during HC-SCR. Also in NH_3-SCR, $Ag_n^{\delta+}$ clusters have been identified as key sites in the SCR reaction [32, 34]. Moreover, Figure 4.5 shows the deconvoluted spectra of the Ag/Al_2O_3 sample pretreated in an SCR mixture of NO, NH_3 and O_2 (Ar-bal). It is clear that peaks in the region assigned to isolated Ag^+ ions (200-260 nm) increase in this oxidizing environment. Comparing the spectra, it can be seen that peaks in the wavelength range assigned to $Ag_n^{\delta+}$ clusters that still are present after the treatment at 200°C, have disappeared after the exposure at 300°C. This implies that when hydrogen is present in the gas-phase environment, silver clusters are conserved at higher temperatures, which might be an important function of hydrogen in NH_3-SCR. This is in accordance with the reaction mechanism suggested for NH_3-SCR by Shimizu and Satsuma [32]: *i*) dissociation of H_2 on the Ag site, *ii*) spillover of the H atom to form a proton on Al_2O_3, *iii*) aggregation of isolated Ag^+ ions to $Ag_n^{\delta+}$-clusters ($n \leq 8$), *iv*) reduction of O_2 under the cooperation of $Ag_n^{\delta+}$-clusters and H^+ to O_2^-, H_2O and $Ag_n^{\delta+}$ or Ag^+, *v*) N-H activation by O_2^- to yield NH_x ($x \leq 2$) *vi*) oxidation of NO by O_2^- forming NO_2 and *vii*) reaction between NH_x and NO to yield N_2 and H_2O. A study by Tamm et al. [75], confirms that silver is needed for the dissociation of H_2 which directly participates in the mechanism and also that the NO to NO_2 oxidation is part of the reaction mechanism.

4.1.2 Effect of the reductant dosage

The reductant in NH_3-SCR is typically supplied from urea, which decomposes to ammonia over the catalyst, see Figure 4.6 for a schematic illustration of a

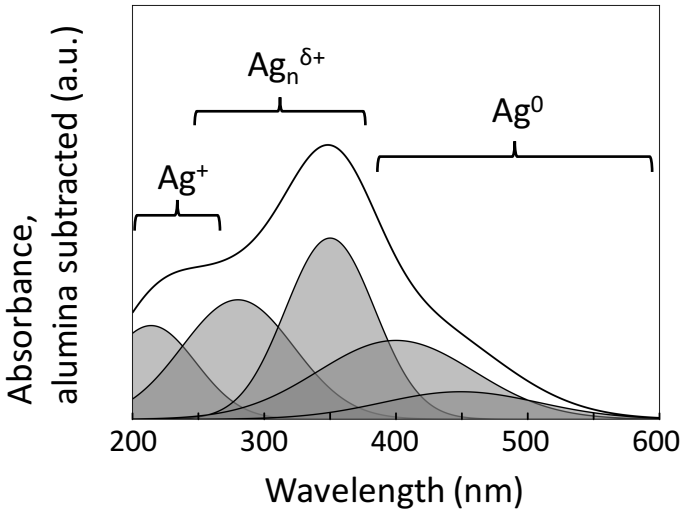

Figure 4.2: Alumina-subtracted UV-vis spectrum of the fresh Ag/Al_2O_3 sample with peak intervals assigned to isolated Ag^+-ions, $Ag_n{}^{\delta+}$-clusters and Ag^0.

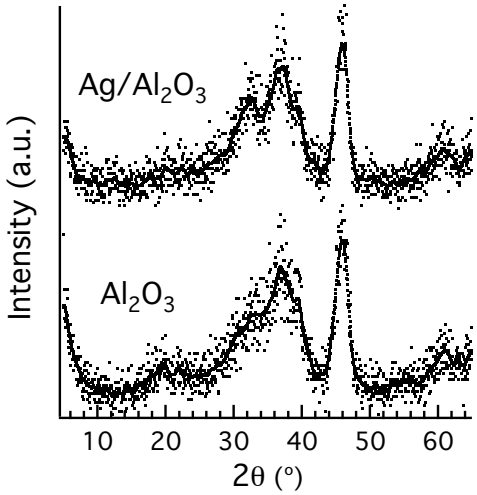

Figure 4.3: XRD patterns of the Ag/Al_2O_3 and γ-Al_2O_3 samples. The solid line represents the floating median of the intensity in the diffractograms.

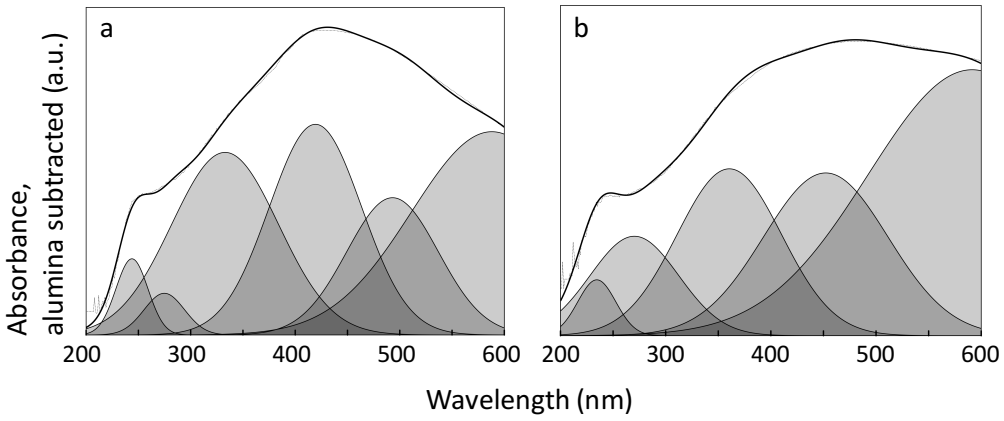

Figure 4.4: Alumina-subtracted UV-vis spectra of the Ag/Al_2O_3 sample pretreated in H_2 at a) 200°C and b) 300°C.

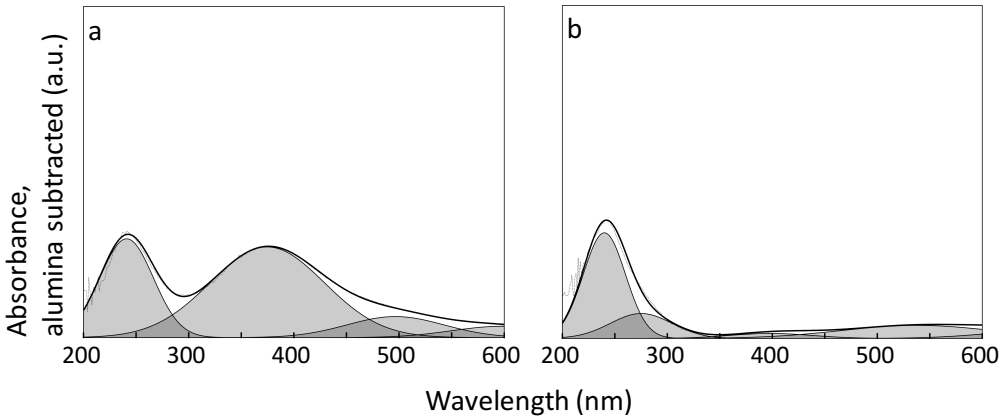

Figure 4.5: Alumina-subtracted UV-vis spectra of the Ag/Al_2O_3 sample pretreated in an SCR mixture of NO, NH_3 and O_2 at a) 200°C and b) 300°C.

urea-SCR system. However, optimizing the spray setup is difficult and may result in uneven ammonia distribution, causing inefficient NO_x conversion and ammonia slip. A quantification and analysis of this issue is addressed in Paper III.

The degree of uneven distribution of ammonia to each individual catalyst channel in a hydrogen-assisted NH_3-SCR Ag/Al_2O_3 catalyst is evaluated for two different cases; with the injection spray situated in the center of the exhaust pipe or at the pipe wall. In this study, the results of the computational fluid dynamics (CFD) simulation by Lundström and Ström [76] were combined with a kinetic model developed by Tamm et al. [33], adapted to new experimental data. Gaussian probability distribution functions for the two cases of ammonia dosage are shown in Figure 4.7, where the probability that a catalyst channel receives a certain ammonia dose is plotted versus the range of doses seen in the raw data. The ammonia dose is here normalized by the average dose, so that an ammonia dose of two indicates that the channel in question receives twice the amount of ammonia that the average channel does. It is clear that the arrangement with the spray positioned in the center of the exhaust pipe produces more evenly distributed ammonia to the inlet of the catalyst than the arrangement with the spray originating from the exhaust pipe wall. However, both arrangements produce a large spread in the dose to the individual channel.

Figure 4.8 shows the NO conversion and the ammonia slip as functions of the normalized ammonia dose. These are calculated with the kinetic model using the input parameters of the Ag/Al_2O_3 catalyst described previously. It is assumed that an average dose implies dosing 500 ppm NH_3 (and 1000 ppm H_2) to reduce the 500 ppm NO, which is consistent with the fact that the global stoichiometry between NO:NH_3:H_2 is 1:1:2 during the SCR reactions [31]. The NO conversion increases rapidly with increasing dose from zero to unity, and then it increases another 10 percentage points up to a dose of approximately four times the average, after which no further improvement in NO conversion is observed with increasing ammonia dosage. However, the ammonia slip increases almost linearly above an ammonia dose equal to unity and reaches more than 4500 ppm for a channel that receives 10 times the average ammonia dose. For doses lower than unity, the ammonia slip is insignificant.

The average NO conversions and ammonia slips for the two spray arrangements depicted in Figure 4.7 are shown in Table 4.1. These values are calculated with the micro-kinetic model for the distribution of channel inlet conditions seen in the raw CFD data. It is shown that the global NO conversion is higher with the more evenly distributed ammonia concentration obtained for the centered spray arrangement. The largest differences are

Position	**NO conversion** [%]	**NH_3 slip** [ppm]	**NO + NH_3 slip** [ppm]
Center	61	300	495
Wall	52	565	805

Table 4.1: NO conversion, NH_3 slip and the sum of NO and NH_3 slip (mean values) as a function of the urea-spray position.

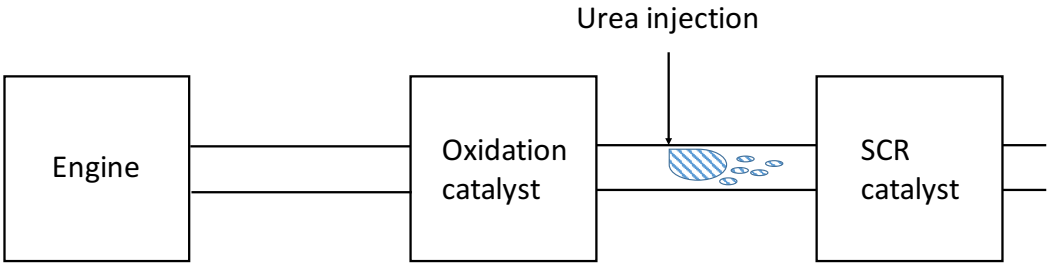

Figure 4.6: Illustration of a simplified diesel aftertreatment system with urea-SCR.

however observed for the ammonia slip, where the effect of local overdosing in the wall spray arrangement becomes apparent.

Although the NO reduction is almost maximized at stoichiometric conditions of NO and ammonia, the optimal ammonia dose is 0.83, as shown in Figure 4.9. In this illustration, it has been assumed that the environmental and health costs for releasing these two pollutants are weighted equally. This information is of importance when designing a urea-SCR system where an additional oxidation catalyst is not used, for example due to lack of space or when there is an increased risk of catalyst poisoning. In these cases, a sub-stoichiometric ammonia dose could be preferable to minimize the risk for ammonia slip.

4.1.3 Influence of the active phase on the lean NO_x reduction

In order to investigate the role of silver for alumina-supported lean NO_x reduction systems, an alumina-supported indium catalyst was prepared in the same way as the Ag/Al_2O_3 and with the equivalent molar amount of active phase (corresponding to an In-loading of 2.1 %wt). After impregnation, the specific surface area of the In/Al_2O_3 sample remained high (188 compared to 197 m^2/g for bare Al_2O_3), as for the Ag/Al_2O_3 sample. XRD diffractograms confirm that also the In/Al_2O_3 sample is similar to the bare γ-Al_2O_3 sample. As shown in Figure 4.10, all peaks are characteristic for γ-Al_2O_3, indicating

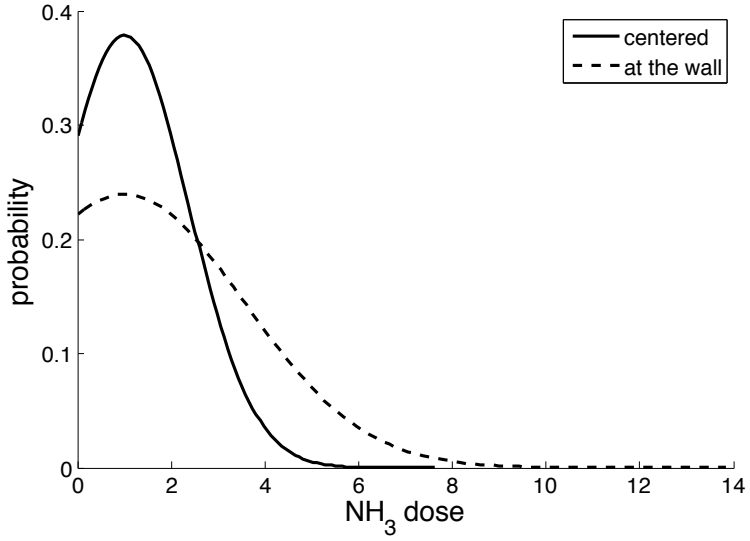

Figure 4.7: Probability distribution function of the NH_3 dose, where a NH_3 dose equal to 1 represents the stoichiometric dose.

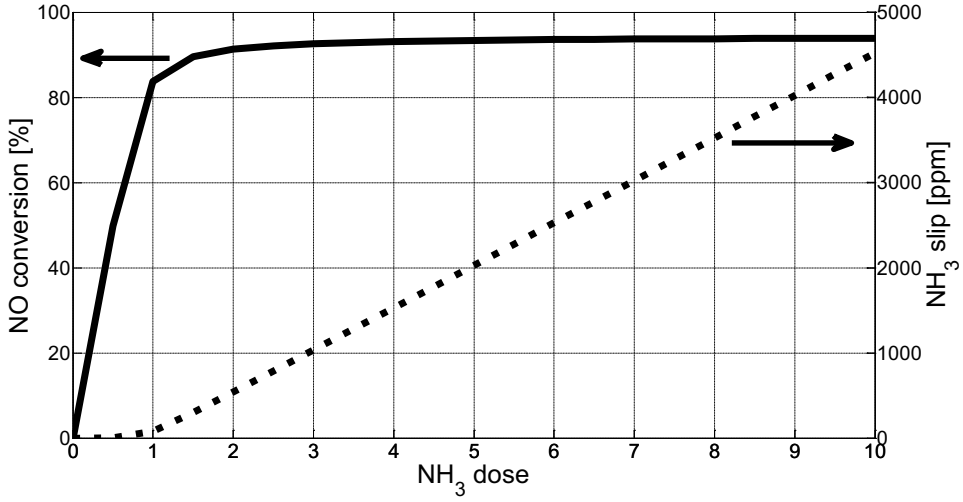

Figure 4.8: NO conversion (left axis) and NH_3 slip (right axis) as a function of the NH_3 dose in an individual catalyst channel at 300°C.

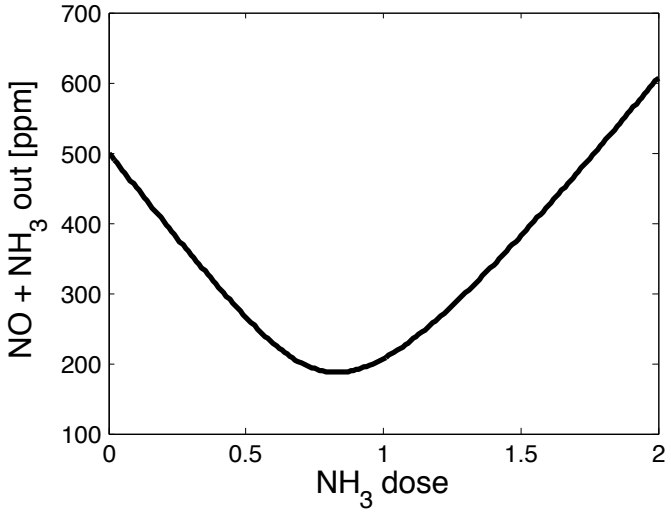

Figure 4.9: The sum of NO and ammonia slip as a function of the normalized ammonia dose to each channel.

that no particles larger than 3-5 nm of other crystalline phases than γ-Al_2O_3 are present in the sample. This catalyst is compared to the Ag/Al_2O_3 catalyst for HC-SCR in Paper I and NH_3-SCR in Paper II.

The activity of In/Al_2O_3 as an SCR catalyst is shown in Figure 4.11. Compared to Ag/Al_2O_3, this catalyst exhibits in general a lower degree of NO_x reduction. However, In/Al_2O_3 reduces NO_x significantly much more efficient with DME compared to the Ag/Al_2O_3 sample, which was totally inactive for this reduction, as shown in Figure 4.2. It has been reported by Tamm et al. [77] that DME undergoes gas-phase radical reactions with NO, O_2 and H_2O, which changes the gas-phase composition considerably before reaching the catalyst. A catalyst suited for DME-SCR should therefore hold other properties than HC-SCR catalysts for non-oxygenated hydrocarbons. One reason that Ag/Al_2O_3 is not suitable as DME-SCR catalyst, could be its oxidizing properties, which may totally oxidize DME. Moreover, the NH_3-TPD experiment shown in Figure 4.12 demonstrates that the In/Al_2O_3 sample holds a higher concentration of acidic sites, compared to the Ag/Al_2O_3 sample. It has been reported that catalysts that exhibit a high concentration of weak acidic sites are more efficient in DME-SCR [78]. The experiment also shows that bare Al_2O_3 exhibits an even higher number of acidic sites than In/Al_2O_3. However, Erkfeldt et al. [74] demonstrated that In/Al_2O_3 shows higher activity for NO_x reduction with DME, compared to In_2O_3 or Al_2O_3 alone. The authors suggest that this is owing to that In_2O_3 consumes

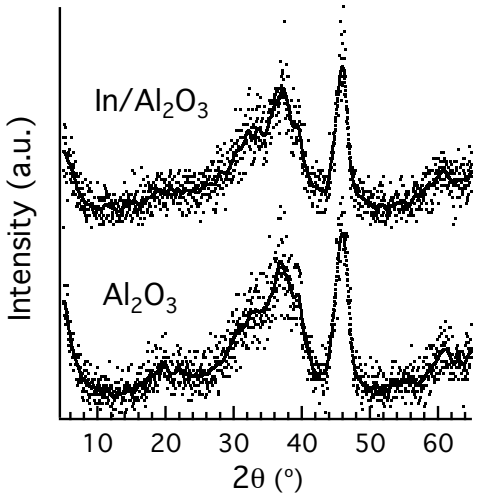

Figure 4.10: XRD patterns of the In/Al_2O_3 and γ-Al_2O_3 samples. The solid line represents the floating median of the intensity in the diffractograms.

a species that otherwise inhibits the reaction, resulting in a more efficient reaction path, or perhaps the formation of additional or more active reaction sites for the combined In/Al_2O_3 compared to the bare oxide.

In addition to Ag/Al_2O_3, In/Al_2O_3 also exhibits a promoting effect when adding hydrogen. This is especially obvious with ethane and ammonia as reductants, as shown in Figure 4.11. The UV-vis spectra of fresh and hydrogen-pretreated In/Al_2O_3 are shown in Figure 4.13. Peaks in the range 200-450 nm are attributed to In_2O_3, according to Refs. [79-84]. After pretreatment in hydrogen, peaks increase at longer wavelengths, i.e. >450 nm, especially after the pretreatment at 200°C. This indicates that the exposure of In/Al_2O_3 to hydrogen results in increased concentrations of species that are more reduced than In_2O_3, which could explain the promoting effect of hydrogen during NH_3-SCR. However, the spectra also experience redshift and broadening of absorbance edges, especially after the pretreatment at 300°C, in the wavelength range 200-300 nm. This indicates increased concentration of In_2O_3 [79]. Park et al. [57] propose that dispersed In_2O_2 clusters promote activation (i.e. partial oxidation) of HC that, with utilization of active alumina sites, selectively reduce NO_x to N_2. Hence, the promoting effect of hydrogen in HC-SCR could originate in increased formation of dispersed In_2O_3 clusters that, in turn, enable HC activation.

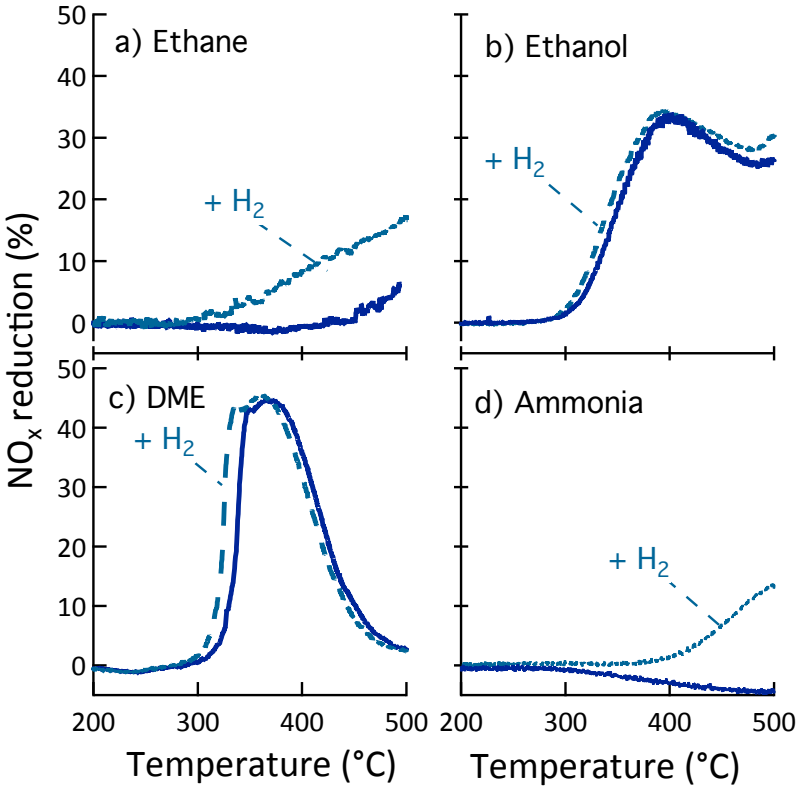

Figure 4.11: Lean NO_x reduction over In/Al_2O_3 as a function of the catalyst temperature using (a) ethane, (b) ethanol, (c) DME (1500 ppm HC-reductant) and (d) ammonia (500 ppm), as the reductant. Gas feed concentrations (except for the reductant): 500 ppm NO, 10% O_2, 5% H_2O, Ar-balance. Dotted lines represent the addition of 1000 ppm H_2 to the gas feed.

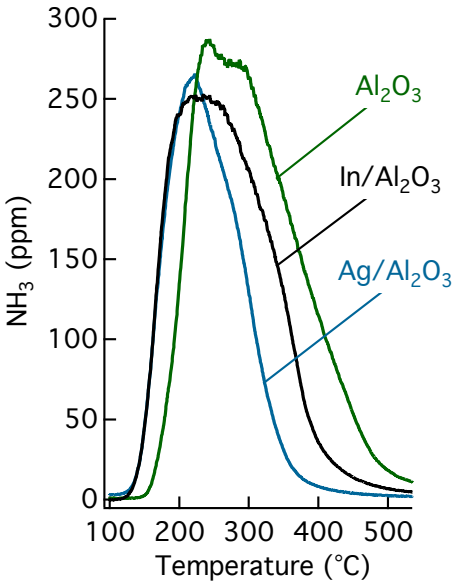

Figure 4.12: NH_3-TPD profiles for the Ag/Al_2O_3, In/Al_2O_3 and bare γ-Al_2O_3 samples.

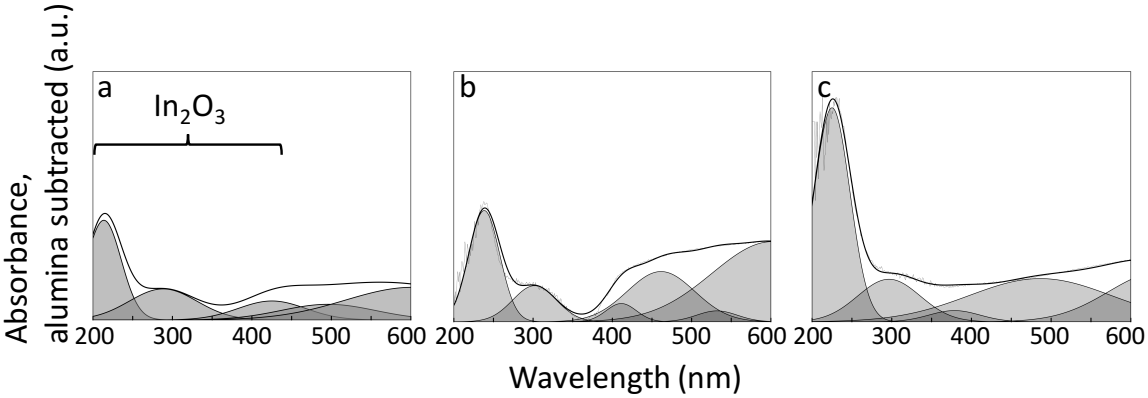

Figure 4.13: Alumina-subtracted UV-vis spectra of In/Al_2O_3 showing a) fresh sample, b) pretreated in H_2 at 200 °C and c) in 300°C.

Chapter 5

Conclusions and future outlook

Ag/Al_2O_3 has been evaluated as SCR catalyst with C_2-hydrocarbons and oxygenates, as well as ammonia, in order to investigate the active sites and the influence of the structure of the reducing agent during lean NO_x reduction. Furthermore, this catalyst was compared to an In/Al_2O_3 catalyst, containing the equivalent molar amount of active phase in order to elucidate the role of the active phase. The connections between the gas-phase environment and type of silver and indium species in the samples were investigated using UV-vis spectroscopy after various gas-phase pretreatments. Furthermore, the consequence of the reductant dosage over Ag/Al_2O_3 was investigated by combining CFD simulations, kinetic modeling and experiments.

The results from the SCR experiments show that the Ag/Al_2O_3 catalyst in general exhibits superior activity for NO_x reduction compared to In/Al_2O_3. However, In/Al_2O_3 shows significantly higher activity with DME as the reductant, which may be explained by gas-phase radical formation that DME experiences together with the more pronounced ability of HC activation (i.e. partial oxidation) that Ag/Al_2O_3 exhibits. The 'hydrogen effect' observed over the Ag/Al_2O_3 sample may be explained by modification of surface species acquired after hydrogen exposure, resulting in increased concentration of $Ag_n^{\delta+}$-clusters. Such clusters have previously been identified as key components in the reaction mechanisms, both during HC- and NH_3-SCR. Furthermore, the results show that in addition to Ag/Al_2O_3, In/Al_2O_3 also exhibits a 'hydrogen effect' during both HC- and NH_3-SCR. Hydrogen exposure of In/Al_2O_3 results in an increased number of In_2O_3 species, which has been identified as an active component for HC activation during HC-SCR. However, more reduced species are also formed during hydrogen exposure, which may be an explanation of the promoting effect of hydrogen during NH_3-SCR over this catalyst. Moreover, the hydrogen effect has been shown to be rapidly reversible when the hydrogen is removed from the gas feed. It

is likely that the origin of this phenomenon is dual and a direct participation of hydrogen in the NO_x reduction reaction mechanism is feasible.

Quantification of the NO reduction and ammonia slip in different locations of the reductant injection spray shows that the probability of an ammonia dose equal to unity is higher when the spray is positioned in the center of the exhaust pipe, compared to at the pipe wall. However, both arrangements produce a large spread in the ammonia dose to the individual catalyst channels. Furthermore, the NO conversion increases rapidly with increasing ammonia dose from zero to unity, and then it increases another 10 percentage points up to a dose of approximately four times the average, after which no further improvement in NO conversion is observed with increasing ammonia dosage. However, the ammonia slip increases almost linearly above an ammonia dose equal to unity and reaches more than 4500 ppm for a channel that receives 10 times the average ammonia dose. For doses lower than unity, the ammonia slip is insignificant.

As a next step, a better understanding of the catalytic sites during reaction conditions could be achieved by studying the construction of nitrogen- and hydrocarbon species on the catalyst surface. A technique useful for this is in-situ FTIR spectroscopy. Also, in-situ diffuse reflectance UV-vis spectroscopy could contribute to a deeper understanding of the surface species interplay during reaction conditions.

Acknowledgements

This work has been funded by the Swedish Research Council and was performed within the Competence Centre for Catalysis, which is hosted by Chalmers University of Technology and financially supported by the Swedish Energy Agency and the member companies: AB Volvo, ECAPS AB, Haldor Topsøe A/S, Scania CV AB, Volvo Car Corporation AB and Wärtsilä Finland Oy.

I would also like to thank:

Professor Hanna Härelind for giving me the opportunity to do my Ph.D. in this group and for being such an amazing supervisor and a great mentor.

My examiner **Professor Magnus Skoglundh** and co-supervisor **Dr. Per-Anders Carlsson** for all the support and guidance.

Ann Jakobsson for all the administrative help.

Hannes, Marika and **Freddy** for all the help in the help in the beginning of my Ph.D.

Anna and **Alexander** for helping me with experimental techniques.

Emma for being the best office mate and such a good friend.

All former and present colleagues at **TYK** and **KCK** for creating such nice working atmosphere.

My family for all the support.

Last but not least, my husband **Henrik** and our daughter **Tove** for making me so happy. I love you!

Bibliography

[1] U.S.E.P. Agency, Clean air act requirements and history, http://www.epa.gov, recieved 2015-08-13.

[2] I. Chorkendorff, J.W. Niemantsverdriet, Concepts of modern catalysis and kinetics, WILEY-VCH Verlag GmbH & Co. KGaA, Weinheim, 2007.

[3] Eurostat Emissions of nitrogen oxides by source sector, ec.europa.eu/eurostat Accessed 2015-08-13.

[4] Dieselnet, http://www.dieselnet.com, Accessed 2015-12-03

[5] K. Arve, L. Capek, F. Klingstedt, K. Eranen, L.E. Lindfors, D.Y. Murzin, J. Dedecek, Z. Sobalik, B. Wichterlova, Top. Catal. 30-1 (2004) 91-95.

[6] J.P. Breen, R. Burch, C. Hardacre, C.J. Hill, J. Phys. Chem. B 109 (2005) 4805-4807.

[7] J.P. Breen, R. Burch, Top. Catal. 39 (2006) 53-58.

[8] H. Kannisto, H.H. Ingelsten, M. Skoglundh, J. Mol. Catal. A: Chem. 302 (2009).

[9] T. Miyadera, Appl. Catal., B. 16 (1998) 155-164.

[10] T. Nakatsuji, R. Yasukawa, K. Tabata, K. Ueda, M. Niwa, Appl. Catal., B. 17 (1998) 333-345.

[11] P. Granger, V.I. Parvulescu, Chem. Rev. 111 (2011) 3155-3207.

[12] M. Bowker, The Basis and Applications of Heterogeneous Catalysis, Oxford Science Publications, 1998.

[13] M.V. Twigg, Catal. Today 163 (2011) 33-41.

[14] R. Burch, Catal. Rev. -Sci. Eng. 46 (2004) 271-333.

[15] Z.M. Liu, S.I. Woo, Catal. Rev. -Sci Eng 48 (2006) 43-89.

[16] W.S. Epling, L.E. Campbell, A. Yezerets, N.W. Currier, J.E. Parks, Catal. Rev. -Sci. Eng. 46 (2004) 163-245.

[17] S. Matsumoto, Y. Ikeda, H. Suzuki, M. Ogai, N. Miyoshi, Appl. Catal., B. 25 (2000) 115-124.

[18] R. Burch, J.P. Breen, F.C. Meunier, Appl. Catal., B. 39 (2002) 283-303.

[19] R. Brosius, K. Arve, M.H. Groothaert, J.A. Martens, J. Catal. 231 (2005) 344-353.

[20] T. Maunula, Y. Kintaichi, M. Inaba, M. Haneda, K. Sato, H. Hamada, Appl. Catal., B. 15 (1998).

[21] K. Eranen, F. Klingstedt, K. Arve, L.E. Lindfors, D.Y. Murzin, J. Catal. 227 (2004) 328-343.

[22] K. Shimizu, J. Shibata, H. Yoshida, A. Satsuma, T. Hattori, Appl. Catal., B. 30 (2001).

[23] K. Shimizu, A. Satsuma, Phys. Chem. Chem. Phys. 8 (2006) 2677-2695.

[24] V.A. Sadykov, S.L. Baron, V.A. Matyshak, G.M. Alikina, R.V. Bunina, A.Y. Rozovskii, V.V. Lunin, E.V. Lunina, A.N. Kharlanov, A.S. Ivanova, S.A.

[25] K. Shimizu, M. Takamatsu, K. Nishi, H. Yoshida, A. Satsuma, T. Tanaka, S. Yoshida, T. Hattori, J. Phys. Chem. B 103 (1999).

[26] F.C. Meunier, J.P. Breen, V. Zuzaniuk, M. Olsson, J.R.H. Ross, J. Catal. 187 (1999) 493-505.

[27] C. Ciardelli, I. Nova, E. Tronconi, D. Chatterjee, T. Burkhardt, M. Weibel, Chem. Eng. Sci. 62 (2007) 5001-5006.

[28] K.-i. Shimizu, A. Satsuma, Appl. Catal., B. 77 (2007) 202-205.

[29] F. Klingstedt, K. Arve, K. Eranen, D.Y. Murzin, Acc. Chem. Res. 39 (2006).

[30] T. Miyadera, Appl. Catal., B. 2 (1993) 199-205.

[31] S. Tamm, S. Fogel, P. Gabrielsson, M. Skoglundh, L. Olsson, Appl. Catal., B. 136 (2013) 168-176.

[32] K.-i. Shimizu, A. Satsuma, J. Phys. Chem. C 111 (2007) 2259-2264.

[33] S. Tamm, L. Olsson, S. Fogel, P. Gabrielsson, M. Skoglundh, AIChE J. 59 (2013) 4325-4333.

[34] L. Yu, Q. Zhong, S. Zhang, Phys. Chem. Chem. Phys. 16 (2014) 12560-12566.

[35] L. Zhang, C. Zhang, H. He, J. Catal. 261 (2009) 101-109.

[36] K. Masuda, K. Tsujimura, K. Shinoda, T. Kato, Appl. Catal., B. 8 (1996).

[37] T. Miyadera, Appl. Catal., B. 13 (1997) 157-165.

[38] H. Harelind, F. Gunnarsson, S.M.S. Vaghefi, M. Skoglundh, P.-A. Carlsson, ACS Catal 2 (2012) 1615-1623.

[39] T.E. Hoost, R.J. Kudla, K.M. Collins, M.S. Chattha, Appl. Catal., B. 13 (1997) 59-67.

[40] L.E. Lindfors, K. Eranen, F. Klingstedt, D.Y. Murzin, Top. Catal. 28 (2004) 185-189.

[41] T. Chaieb, L. Delannoy, G. Costentin, C. Louis, S. Casale, R.L. Chantry, Z.Y. Li, C. Thomas, Appl. Catal., B. 156 (2014) 192-201.

[42] N. Bogdanchikova, F.C. Meunier, M. Avalos-Borja, J.P. Breen, A. Pestryakov, Appl. Catal., B. 36 (2002) 287-297.

[43] J. Shibata, Y. Takada, A. Shichi, S. Satokawa, A. Satsuma, T. Hattori, J. Catal. 222 (2004) 368-376.

[44] S. Satokawa, Chem. Lett. (2000) 294-295.

[45] S. Tamm, N. Vallim, M. Skoglundh, L. Olsson, J. Catal. 307 (2013) 153-161.

[46] H. Kannisto, H.H. Ingelsten, M. Skoglundh, Top. Catal. 52 (2009).

[47] N.A. Sadokhina, D.E. Doronkin, G.N. Baeva, S. Dahl, A.Y. Stakheev, Top. Catal. 56 (2013) 737-744.

[48] C. Thomas, Appl. Catal., B. 162 (2015) 454-462.

[49] P.S. Kim, M.K. Kim, B.K. Cho, I.-S. Nam, S.H. Oh, J. Catal. 301 (2013) 65-76.

[50] S. Satokawa, J. Shibata, K. Shimizu, S. Atsushi, T. Hattori, Appl. Catal., B. 42 (2003) 179-186.

[51] R. Burch, J.P. Breen, C.J. Hill, B. Krutzsch, B. Konrad, E. Jobson, L. Cider, K. Eranen, F. Klingstedt, L.E. Lindfors, Top. Catal. 30-1 (2004) 19-25.

[52] D.E. Doronkin, S. Fogel, S. Tamm, L. Olsson, T.S. Khan, T. Bligaard, P. Gabrielsson, S. Dahl, Appl. Catal., B. 113 (2012) 228-236.

[53] J.H. Li, J.M. Hao, X.Y. Cui, L.X. Fu, Catal. Lett. 103 (2005).

[54] M. Boutros, J. Starck, B. de Tymowski, J.-M. Trichard, P. Da Costa, Top. Catal. 52 (2009).

[55] T. Maunula, Y. Kintaichi, M. Haneda, H. Hamada, Catal. Lett. 61 (1999).

[56] M. Haneda, Y. Kintaichi, N. Bion, H. Hamada, Appl. Catal., B. 42 (2003).

[57] P.W. Park, C.S. Ragle, C.L. Boyer, M.L. Balmer, M. Engelhard, D. McCready, J. Catal. 210 (2002) 97-105.

[58] S. Brunauer, P.H. Emmett, E. Teller, J. Am. Chem. Soc. 60 (1938) 309-319.

[59] K.S.W. Sing, Adv. Colloid Interface Sci. 76 (1998) 3-11.

[60] G. Leofanti, M. Padovan, G. Tozzola, B. Venturelli, Catal. Today 41 (1998) 207-219.

[61] J.R. Anderson, K.C. Pratt, Introduction to characterization and testing of catalysts, Academic Press Inc., University of Melbourne, Australia, 1985.

[62] C. Wang-Hansen, C.J. Kamp, M. Skoglundh, B. Andersson, P.-A. Carlsson, J. Phys. Chem. C 115 (2011) 16098-16108.

[63] M. Haneda, E. Joubert, J.C. Menezo, D. Duprez, J. Barbier, N. Bion, M. Daturi, J. Saussey, J.C. Lavalley, H. Hamada, J. Mol. Catal. A: Chem. 175 (2001).

[64] J.A. Perdigon-Melon, A. Gervasini, A. Auroux, J. Catal. 234 (2005).

[65] C. Shi, M.J. Cheng, Z.P. Qu, X.H. Bao, Appl. Catal., B. 51 (2004) 171-181.

[66] S.J. Miao, Y. Wang, D. Ma, Q.J. Zhu, S.T. Zhou, L.L. Su, D.L. Tan, X.H. Bao, J. Phys. Chem. B 108 (2004) 17866-17871.

[67] V.A. Kondratenko, U. Bentrup, M. Richter, T.W. Hansen, E.V. Kondratenko, Appl. Catal., B. 84 (2008) 497-504.

[68] M. Mannikko, M. Skoglundh, H.H. Ingelsten, Appl. Catal., B. 119 (2012).

[69] A. Musi, P. Massiani, D. Brouri, J.-M. Trichard, P. Da Costa, Catal. Lett. 128 (2009) 25-30.

[70] A.N. Pestryakov, A.A. Davydov, J. Electron Spectrosc. Relat. Phenom. 74 (1995) 195-199.

[71] M. Richter, R. Fricke, R. Eckelt, Catal. Lett. 94 (2004) 115-118.

[72] K. Sato, T. Yoshinari, Y. Kintaichi, M. Haneda, H. Hamada, Appl. Catal., B. 44 (2003) 67-78.

[73] X. She, M. Flytzani-Stephanopoulos, J. Catal. 237 (2006).

[74] S. Erkfeldt, M. Petersson, A. Palmqvist, Appl. Catal., B. 117 (2012) 369-383.

[75] S. Tamm, Catal. Lett. 143 (2013) 957-965.

[76] A. Lundström, H. Ström, In:Sprays: Types, Technology and Modeling Vella, M.C., Nova Science Publishers (ISBN: 978-161324345-9), 2011.

[77] S. Tamm, H.H. Ingelsten, M. Skoglundh, A.E.C. Palmqvist, Appl. Catal., B. 91 (2009).

[78] S.G. Masters, D. Chadwick, Appl. Catal., B. 23 (1999) 235-246.

[79] J. Lv, T. Kako, Z. Li, Z. Zou, J. Ye, J. Phys. Chem. C 114 (2010) 6157-6162.

[80] X. Yang, J. Xu, T. Wong, Q. Yang, C.-S. Lee, Phys. Chem. Chem. Phys. 15 (2013) 12688-12693.

[81] G. Zhu, L. Guo, X. Shen, Z. Ji, K. Chen, H. Zhou, Sens. Actuators B 220 (2015) 977-985.

[82] F. Zhang, X. Li, Q. Zhao, Q. Zhang, M. Tade, S. Liu, J. Colloid Interface Sci. 457 (2015) 18-26.

[83] J.Z. Yin, S.B. Huang, Z.C. Jian, M.L. Pan, Y.Q. Zhang, Z.B. Fei, X.R. Xu, Appl. Phys. A 120 (2015) 1529-1535.

[84] Q. Liu, W. Zhang, R. Liu, G. Mao, Eur. J. Inorg. Chem. (2015) 845-851.